THE JOURNAL OF COMPARATIVE NEUROLOGY 488:369–383 (2005)

Structure and Function Relationship in the Abdominal Stretch Receptor Organs of the Crayfish

NUHAN PURALI*
Hacettepe University, Medical Faculty, Department of Biophysics, Sihhiye, 06100 Ankara, Turkey

ABSTRACT

The structure/function relationship in the rapidly and slowly adapting stretch receptor organs of the crayfish (*Astacus leptodactylus*) was investigated using confocal microscopy and neuronal modeling methods. Both receptor muscles were single muscle fibers with structural properties closely related to the function of the receptors. Dendrites of the rapidly adapting neuron terminated in a common pile of nerve endings going in all directions. Dendrites of the slowly adapting neuron terminated in a characteristic *T* shape in multiple regions of the receptor muscle. The slowly adapting main dendrite, which was on average 2.1 times longer and 21% thinner than the rapidly adapting main dendrite, induced larger voltage attenuation. The somal surface area of the slowly adapting neuron was on average 51% larger than that of the rapidly adapting neuron. Variation in the neuronal geometry was greatest among the slowly adapting neurons. A computational model of a neuron pair demonstrated that the rapidly and the slowly adapting neurons attenuated the dendritic receptor potential like low-pass filters with cut-off frequencies at 100 and 20 Hz, respectively. Recurrent dendrites were observed mostly in the slowly adapting neurons. Voltage signals were calculated to be propagated 23% faster in the rapidly adapting axon, which is 51% thicker than the slowly adapting axon. The present findings support the idea that the morphology of the rapidly and the slowly adapting neurons evolved to optimally sense the dynamic and the static features of the mechanical stimulus, respectively. J. Comp. Neurol. 488:369–383, 2005.

Indexing terms: mechanoreceptor; receptor muscle; receptor neuron; morphology; confocal microscopy; neuronal modeling

Crustacean abdominal stretch receptor organs have perhaps been the most common primary mechanoreceptor preparation since they were first described by Alexandrowicz (1951). The organ in situ is relatively easy to identify and prepare for many types of electrophysiological and pharmacological experiments which may not be possible in any other preparation. These properties of the preparation prompted several pioneering studies on the mechanotransduction, excitability, and synaptic inhibitory mechanisms (for review, see Swerup and Rydqvist, 1992; Purali, 1997). Furthermore, the presence of two closely positioned mechanoreceptors with different adaptive properties makes it a unique preparation for studying mechanisms of adaptation. In a series of studies, the viscoelastic properties of the receptor muscles (Rydqvist et al., 1990, 1994), properties of the neuronal potassium current (Rydqvist and Purali, 1991; Purali and Rydqvist, 1992), transducer current (Rydqvist and Purali, 1993), sodium current (Purali and Rydqvist, 1998), and the firing properties of the receptor neurons (Purali, 2002) have been investigated comparatively in the rapidly and slowly adapting receptors to explore the cause(s) of adaptation (Purali, 1997). However, up to the present there has been no study investigating the relationship between the mor-

Grant sponsor: Hacettepe University Research Fund; Grant number: 0102101003; Grant sponsor: Research Council of Turkey; Grant number: AYD-287; Grant number: DPT (98K-121670).

*Correspondence to: Nuhan Purali, Hacettepe University, Medical Faculty, Department of Biophysics, Sihhiye, 06100 Ankara, Turkey.
E-mail: npurali@hacettepe.edu.tr

Received 11 November 2004; Revised 19 January 2005; Accepted 25 February 2005

DOI 10.1002/cne.20590

Published online in Wiley InterScience (www.interscience.wiley.com).

phology of the receptors and the reported differences in the receptor responses.

The intracellular microinjection technique, allowing a specific labeling and differential imaging of the neurons and muscle fibers, was used for the first time in the present work. Using confocal microscopy and digital image processing methods in live preparations, 3D images of the receptor muscles, neurons, and subcellular structures were obtained. Physical dimensions of the neuronal structures were measured and the corresponding electrotonic parameters calculated. These values were inserted into a computational neuron model simulating passive propagation of the receptor potential through the dendritic tree. Images and computed receptor responses were comparatively discussed with regard to the physiological function of the rapidly and the slowly adapting receptors.

MATERIALS AND METHODS

Preparation

Rapidly and slowly adapting stretch receptor organs were dissected from the first to fourth abdominal segments of the crayfish, *Astacus leptodactylus*, as previously described (Purali, 2002). Dissected receptor organs were mounted in their original orientation in a recording chamber and perfused in the control solution. The bottom of the chamber was a coverglass. The surface of the coverglass was the *X-Y* plane and the *Z* axis was perpendicular to that (see Fig. 2A). The composition of the control solution was (in mM): 200 NaCl, 5.4 KCl, 13.5 $CaCl_2$, 2.6 $MgCl_2$ (van Harreveld, 1936) and buffered to pH 7.4 using 10 mM HEPES. In the majority of the experiments, one or more microelectrodes were inserted into the receptor neurons or muscle fibers to load the fluorescent dyes. An amplifier (EPC-8, Heka, Germany) was used for membrane potential recording and current injection. In some experiments, fluorescent dyes were injected into cells through an intracellular microelectrode (using a pneumatic pico-pump; PV-830, WPI, Sarasota, FL). In the handling of the experimental animals, national guidelines were followed and approval from the Hacettepe University Ethics Committee was obtained.

Fluorescent labeling and imaging

In the majority of the experiments polar fluorescent tracers, Alexa-hydrazide 488 or 568, were used for imaging the cell morphology. Dyes were loaded into the neurons by passing a constant negative current via an intracellular microelectrode filled with 10 mM dye solution in 200 mM KCl (Purali, 2002). However, the dyes were pressure-injected into the muscle fibers. Myofibrils of the receptor muscle fibers were imaged by using a fluorescent conjugate of the F-actin specific mushroom toxin, phalloidin (Waterman-Storer et al., 2000). The preparation was fixed in 3.7% paraformaldehyde (in 100 mM PBS, pH 7.4) solution for 10 minutes followed by a permeabilization in 0.1% Triton X-100 (in 100 mM PBS, pH 7.4) solution for 5 minutes. The preparation was washed 3–4 times in PBS and incubated in 165 nM Alexa Fluor 546 phalloidin for 20 minutes at room temperature. After washing in PBS, the preparation was mounted in a 1:1 solution of PBS and glycerol. Oregon green 488 conjugated paclitaxel was used to label the tubulin filaments. The preparation was incubated in 20 μM conjugate for 2 hours, followed by several washes in the control solution containing 2% bovine serum albumin (Diaz et al., 2000). The nuclei of the cells in the preparation were labeled by incubating the preparation in 1 μM cell permeable fluorescent cyanine nucleic acid stain, SYTO-Orange (S-11360) (Frey, 1995). Labeled specimens were mounted onto an inverted microscope equipped with a confocal laser scanner (200-M, LSM-Pascal, Zeiss, Germany). 488 and/or 543 nm laser lines from argon and helium-ion lasers were used to excite the fluorescent dyes. Images acquired in various experimental conditions were processed in a 3D LSM (Zeiss, Germany) environment. The same program was used for the processing and production of the photomicrographs. Surface area and volume measurements were performed using a special program developed for confocal image stacks obtained in LSM Pascal confocal microscope (Zeiss, Germany). Briefly, contrast of the sequential images has been enhanced and a subsequent Gauss filter was used for smoothing. An erosion and dilation operation was applied to reduce convex bulges in the contour of the region. The images were segmented as previously described by Schiemann et al. (1992). Finally, the mask image was constructed and surface and/or volume of the object was calculated. Fluorescent probes used in the present study were commercially supplied from Molecular Probes Europe (Leiden, The Netherlands) and the other chemicals were obtained from Sigma (St. Louis, MO).

Neuronal modeling

Raw data about the length, width, volume, and surface area of the receptor neurons or neuron parts were extracted from the stereo and projection images of the neurons. Physical measurements were converted into electrical terms by using some conventional constants and equations: $\tau_m = R_m C_m$; $T = t/\tau_m$; $\lambda = (aR_m/2R_i)^{1/2}$; $X = x/\lambda$; $L = l/\lambda$; *and* $R_\infty = \lambda ri$, where R_m is the specific membrane resistance = 10,000Ω cm^2; R_i is the specific axoplasmic resistance = 65Ω cm; ri is the intracellular resistance per unit length (Ω/cm); C_m is the specific membrane capacitance = 1 μF/cm^2; τ_m is the membrane time constant; λ is the membrane length constant; a is the axonal radius; X is the electrotonic distance; T is the dimensionless variable that is proportional to time; l is the physical length of the cable; L is the electrotonic length; and R_∞ is the input resistance of a λ length of a dendrite.

Whenever applicable, the one-dimensional cable theory was used to analyze electrotonic properties of the neuronal structures (Rall, 1959, 1962). For a *nonisopotential cell (cylinder),* spatial and temporal changes in the membrane potential were expressed by the general form of the cable equation:

$$d^2V_m/dX^2 - dV_m/dT - V_m = 0 \qquad (1)$$

The general solution of the partial differential equation was obtained for some conditions to calculate the voltage attenuation in a homogenous tubular dendrite as a function of time and distance.

The arbitrary branching structure of the neuronal dendrites could not be represented by one-dimensional cable equations. Thus, a compartmental model was constructed to simulate the electrotonic properties of the neurons. The model allowed a realistic simulation of both the actual branching patterns of the dendrites and the calculated

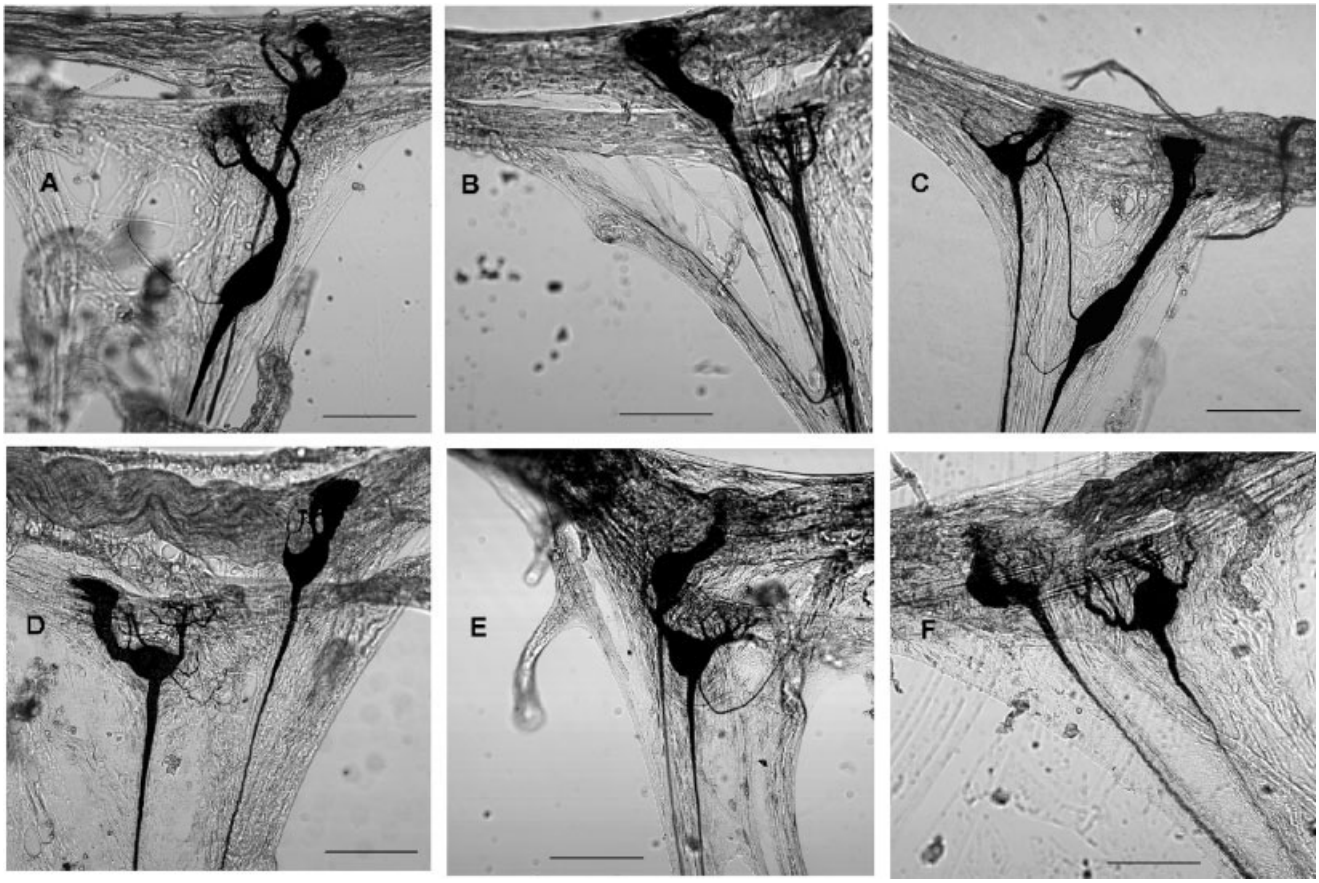

Fig. 1. Various stretch receptor preparations. Fluorescent image of Alexa hydrazide-loaded receptor neurons were subtracted from the picture of the preparation obtained by transmitted light detection mode. Scale bars = 200 μm.

equivalent cable, representing the whole dendritic tree (Koch and Segev, 1998; Johnston and Miao-Sin, 1995). The calculations and the modeling were performed in Matlab-simulink (MathWorks, Natick, MA) environment.

Statistical analysis

The results are expressed as means ± standard error of the means (SEM); n is the number of experiments in the group. The statistical significance of the results was quantified using Student's *t*-test. A $P < 0.05$ was considered statistically significant.

RESULTS

Stretch receptor organ preparation

In the abdominal segments of the crayfish there were a pair of receptor organs on each side. The pair contained one rapidly and one slowly adapting receptor in a closely positioned configuration. Each receptor consisted of a receptor muscle and a bipolar sensory neuron inserting into the receptor muscle with its fine dendrites. Afferent axons extending from the proximal end of the receptor neurons constituted the segmental nerve, together with the efferent axons innervating the receptors. Receptors were covered by a connective tissue. The general structure of the receptor pairs from various segments was similar (Fig. 1).

Receptor muscles

In order to supply some information about the general morphology and the fine structure of the receptor muscles, 26 rapidly and 24 slowly adapting receptor muscles were investigated. The specialized part of the receptor muscles where sensory neuronal dendrites terminate was investigated as an individual compartment. This part is referred to as the neuronal insertion zone (NIZ). Morphological measurements were obtained from the images acquired in the transmitted light detection mode. Muscle compartments were tracked using 3D images of the Alexa-488-injected fibers. Myofibrils and tubulin filaments were labeled by using fluorescent phalloidin and paclitaxel probes, respectively.

Rapidly adapting receptor muscle

The rapidly adapting receptor muscle originated from the cephalic end of an abdominal segment and inserted into the cephalic end of the consecutive segment (Fig. 2A). The muscle was parallel to the cephalo-caudal axis of the animal in situ. The muscle length was related to the size of the segment and varied within the range of 3.3–5.5 mm.

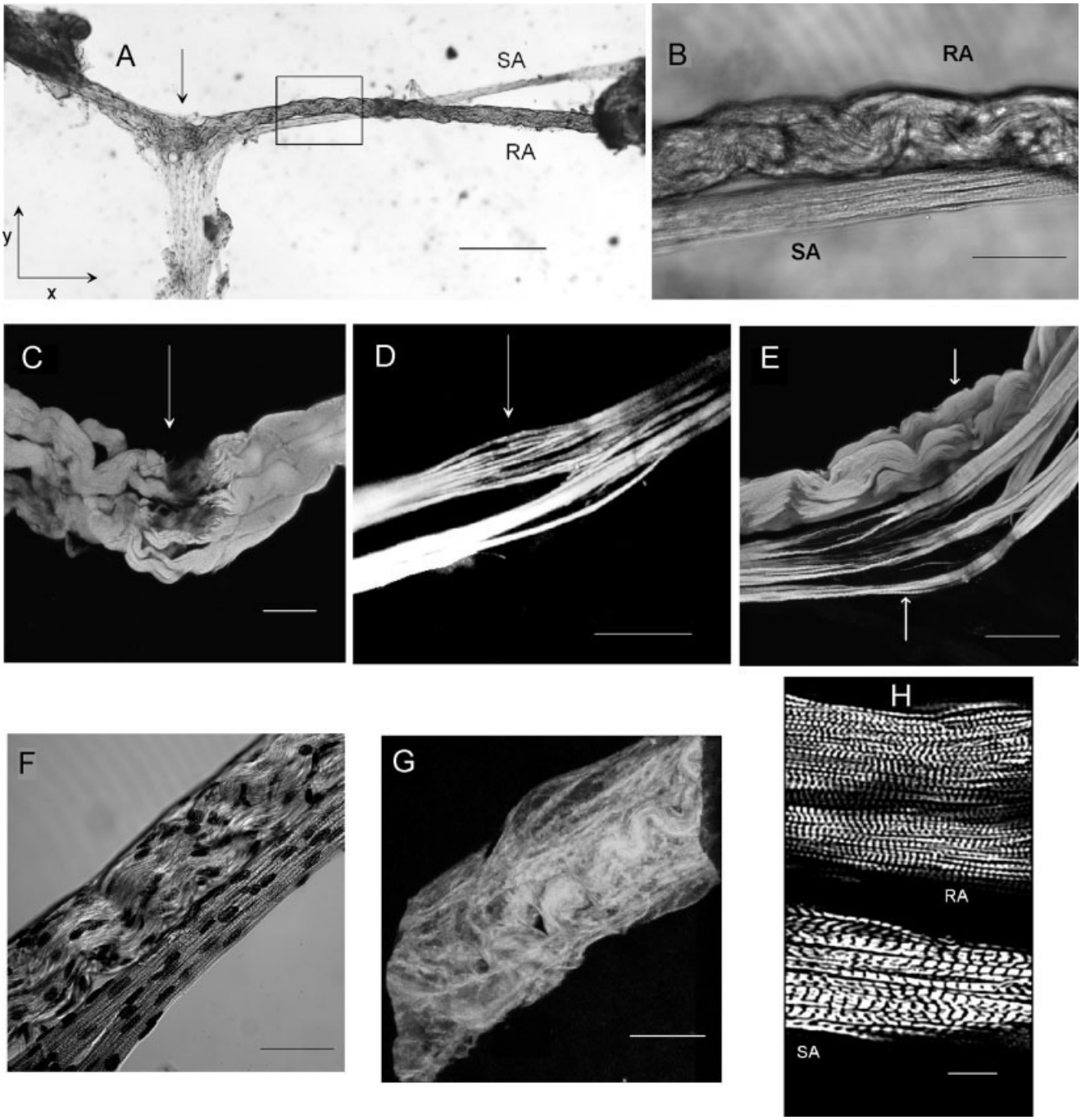

Fig. 2. Receptor muscles obtained under various experimental conditions. **A:** The slowly (SA) and the rapidly adapting (RA) receptor muscles of the preparation acquired by transmitted light detection mode. Arrow indicates the neuronal insertion zone (NIZ). The caudal part is on the left and cephalic part is on the right. **B:** Part of the receptor muscles (shown in the frame in A) at larger magnification. **C,D:** Alexa hydrazide loaded rapidly and slowly adapting receptor muscles, respectively. Arrows indicate the NIZ. **E:** Fluorescently labeled myofibrils of the receptor muscles by using a fluorescent phalloidin probe. Arrows indicate the NIZ. **F:** Nuclei of the rapidly and slowly adapting receptor muscles. Fluorescent picture of the nuclei was subtracted from its pair acquired by transmitted light detection mode. **G:** Fluorescent picture of tubulin filaments of the rapidly adapting receptor muscle. 25° rotated projection image of Oregon green 488 conjugated Paclitaxel-labeled filaments reconstructed from a stack of image sections from a part of the receptor muscle. **H:** Sarcomeres and labeled myofibrils of the rapidly and slowly adapting receptor muscle fibers. A and C–H are seven different preparations. Scale bars = 500 μm in A; 100 μm in B–F; 50 μm in G; 20 μm in H.

The receptor muscle could conceptually be divided into cephalic and caudal parts, in reference to the place where sensory neurons inserted. The caudal part was 40 ± 5% (n = 13, $P = 0.0004$) shorter than the cephalic part (Fig. 2A). The widths of the receptor muscle at the cephalic and caudal parts were 123.8 ± 4.12 and 129.7 ± 6.2 μm (n = 24), respectively (Fig. 2A,B). However, at the receptor neuronal insertion zone, muscle thickness 153.6 ± 9.2 μm was significantly ($P = 0.0095$) larger than that measured at any other part of the muscle (Fig. 2C). Both parts of the fiber were spiral in shape, and had many sarcolemmal invaginations developing gradually into some muscle branches. In the cephalic part of the receptor muscle 2–3 main muscle branches were distinctly observed towards the NIZ. The major branches were subdivided into finer, closely located branches. Some branches inserted into the NIZ, while some passed through it to the caudal part of the receptor muscle (Fig. 2C). The caudal part of the receptor muscle had 3–6 large muscle branches. The fluorescent dye injected into one of the major cephalic muscle branches diffused into its finer branches rapidly but required 0.2–0.5 hours to diffuse into the other neighboring major muscle branches. If sufficient time was given the dye diffused into the caudal part through the NIZ and distributed uniformly within the whole muscle fiber (Fig. 2C).

In fixed and permeabilized preparations it was possible to image the myofibrils by using a fluorescent phalloidin probe. Spiral myofibrils, 0.7–1.3 μm in diameter, lay along the receptor muscle fiber (Fig. 2E). A bundle of 12–31 of the myofibrils made a muscle branch. Sarcomeres, imaged at larger magnifications, were 2.15 ± 0.25 μm in length (n = 6) (Fig. 2H). Spiral organization of the receptor muscle branches was supported by a fine tubulin structure covering the muscle branches, providing connections within the branches (Fig. 2G). A nucleic acid specific probe (Syto-Orange) labeled many cell nuclei in the receptor muscle (Fig. 2F). Those were ovoid in shape with short and long diameters of ~20.6 and 9.3 μm, respectively. Nuclei were uniformly distributed within and between the myofibril bundles of the muscle fiber. About 20 nuclei were counted for each 100 μm length of the receptor muscle.

Slowly adapting receptor muscle

Slowly adapting receptor muscles lay in pairs with the rapidly adapting receptor muscles. The muscle fibers were parallel and adjacent to each other. However, slowly adapting receptor muscle was generally located medially to the rapidly adapting muscle (Fig. 2A,B). The muscle length was usually 2–4% shorter than that of the adjacent rapidly adapting receptor muscle. The caudal part of the muscle was 34 ± 8% shorter than the cephalic part. Ignoring the NIZ, the slowly adapting receptor muscle was flat in shape and had a width of 50.4 ± 2.51 μm (n = 19). However, in the NIZ the muscle fiber was split into 10–16 fine branches and the muscle width increased to 119.7 ± 6.3 μm (n = 19, $P < 0.0001$) (Fig. 2D,E). In the majority of preparations a major branch passed through the NIZ with a slight reduction in width. However, other branches tapered considerably while passing through the NIZ (Figs. 2D, 3C). Towards the NIZ, 2–4 muscle branches were separated from the rest of the branches. They passed the NIZ by curving in the direction of the sensory neuron and joined the other group at the other side (Fig. 3C). In its cross section the fiber was not circular but oval. Thus, in the present work the thickness of the muscle fibers in *X-Y* plane was defined as the width of the fiber instead of its diameter.

Myofibrils were imaged using a fluorescent phalloidin probe. As shown in Figure 2E, 15–24 myofibrils, 0.8–5.8 μm in width, were counted in each receptor muscle fiber. A sarcomere length of 4.61 ± 0.28 μm (n = 6) in the slowly adapting receptor muscle was significantly ($P = 0.0002$) longer than that of the rapidly adapting receptor muscle (Fig. 2H). A nucleic acid-specific fluorescent probe (Syto-Orange) labeled a population of cell nuclei distributed uniformly within the receptor muscle. Spindly nuclei were about 30 and 6.7 μm in length and width, respectively. About 6–10 nuclei were counted for each 100 μm length of the receptor muscle (Fig. 2F).

Sensory neuronal insertion zone

In the present study the part of the muscle where sensory neuronal dendrites terminate is referred to as the NIZ. The general structure of this particular region in both receptor muscles was similar. However, some properties differed substantially. In the rapidly adapting receptor the muscle length of the NIZ was 152.4 ± 9.6 μm. The nonmuscular part of the NIZ was filled by a mass of intercellular material, into which the dendrites of the rapidly adapting neuron terminated in all directions. The mass of intercellular material was located between the spiral curls of the muscle fiber. The majority of muscle branches passed around the dendrite pile through the NIZ with no contact with the receptor neuron (Fig. 3A). However, a few muscle branches inserted onto the edges of the NIZ (Fig. 3B). Thus, a close contact between the endings of the muscle branch and the sensory dendrites was seldom observed. Myofibrils of the continuous and terminating type of muscle branches were similar to those observed in the remainder of the receptor muscle.

Towards the NIZ the slowly adapting receptor muscle repeatedly subdivided into slender muscle branches (Figs. 2D, 3C). Those branches all passed through the NIZ and united progressively in the other part of the muscle. Connective tissue filled the intercellular space. The length of the NIZ, 246.7 ± 22.6 μm, was significantly longer than that of the rapidly adapting muscle ($P = 0.0047$). Furthermore, the increase in the width of the receptor muscle was more pronounced in the slowly adapting neuron. Some fine muscle branches intermingled with the neighboring parallel terminal dendrites of the sensory neuron. However, not all of the muscle branches had a neighboring terminal dendrite. Some branches passed through the NIZ with no detectable contact with any part of the neuron (Fig. 3C), while some dendrites inserted into some parts of the intercellular material with no detectable muscle branch. The width of the myofibril bundles progressively decreased as the muscle fiber divided into branches. However, myofibrils were continuous through the NIZ (Fig. 2D). As can be followed in the 90° rotated image of the labeled myofibrils, a large space surrounded by the muscle branches housed a mass of intercellular filling material into which dendrites of the slowly adapting neuron inserted (Fig. 3D,E). The tubulin structure, supporting the whole preparation, was continuous through the NIZ of both the rapidly and the slowly adapting receptors (Fig. 3F).

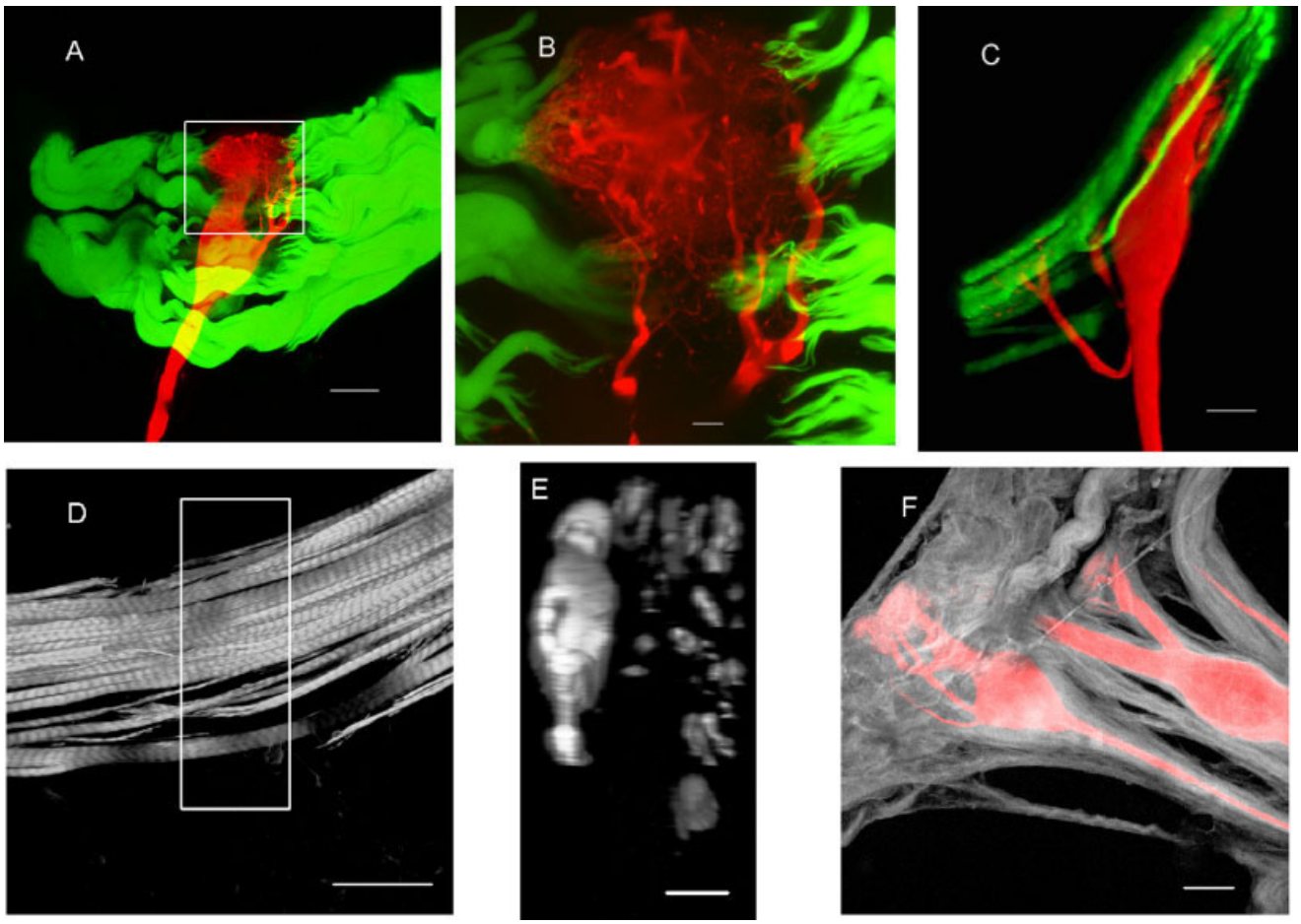

Fig. 3. Various fluorescent pictures of the sensory neuronal insertion zone in the receptor muscles. **A:** Rapidly adapting receptor. Alexa 488 and Alexa 568 hydrazide loaded into the receptor muscle and neuron, respectively. **B:** Section of the preparation (30 μm in height) shown in the frame in A imaged at a larger magnification. **C:** 25° rotated projection image of the slowly adapting receptor. Alexa 488 and Alexa 568 hydrazide loaded into the receptor muscle and neuron, respectively. **D:** Phalloidin-labeled myofibrils in the sensory neuronal insertion zone. **E:** 90° rotated image projection reconstructed from the part shown in frame in D. **F:** Superimposed picture of tubulin filaments (gray) and the receptor neurons (red). Alexa 568 hydrazide iontophoretically loaded into the sensory neurons and preparation subsequently incubated in Oregon green 488 Paclitaxel. In E, *Y* and *Z*, and in the other panels *Y* and *X* are the vertical and horizontal axes, respectively. Scale bars = 100 μm in A,C,D,F; 20 μm in B; 50 μm in E.

Receptor neurons

In the present study morphological measurements were obtained from the images of 73 receptor neurons loaded with a fluorescent cell tracker Alexa-488 or 568. Receptor cells were large peripherally located bipolar neurons. Dendrites extending from the peripheral pole of the soma inserted into the receptor muscles, while a central extension gave the afferent axon joining to the segmental nerve. The general morphology of both neuron types was similar. However, analysis of the images indicated some important qualitative and quantitative differences between the receptor neurons (Fig. 1, Table 1).

Rapidly adapting receptor neuron

The rapidly adapting receptor neuronal soma was located very close to the receptor muscle. In the majority of preparations the soma was observed within the branches of the muscle fiber, and it was not parallel to the *X*-*Y* plane but tilted 10–30° around the *Y* axis (Figs. 1, 3). The somal shape varied considerably within the preparations (Fig. 4). In some preparations (Fig. 4A,D) a large fusiform soma could easily be identified, while a relatively small conical soma (Fig. 4C,G) was observed in other preparations. Another group of neurons had a complex shape where the borders of the soma could hardly be defined (Fig. 4B). The incidence of such somal shapes, independent of the segmental origin of the preparation, was 57, 29, and 14%, respectively. As shown in Figure 4F the neuronal surface was not smooth but had a lot of folding and invaginations. The width of the soma in the *X*-*Y* plane was 67.96 ± 1.85 μm (n = 31) and the height in the *Z* axis was 28.94 ± 1.71 μm (n = 25). Neuronal soma had a volume of $143*10^3 \pm 19*10^3$ μm^3 and a surface area of $32.5*10^3 \pm 2*10^3$ μm^2 (n = 25). Peripheral extensions from the soma gave the main dendrite(s) which existed in three different configurations. In 38% of the neurons the soma tapered into a single, thick main dendrite (Fig. 4D), and in another 24% of the neurons a distinctly observed thick dendrite was

TABLE 1. Comparison of the Physical Properties of the Rapidly and Slowly Adapting Receptor Neurons[1]

	Unit	Rapidly adapting	*n*	Slowly adapting	*n*
Terminal dendrite					
Width	μm	0.59 ± 0.05	19	0.88 ± 0.09	16
Total volume	μm^3	$106*10^3 \pm 13.4*10^3$	18	$112*10^3 \pm 6.4*10^3$	22
Main dendrite					
Width	μm	31.8 ± 1.5	25	26.3 ± 1.4	38**
Length	μm	85.9 ± 6.1	25	179.8 ± 18.1	38***
Surface area	μm^2	$32.9*10^3 \pm 10.6*10^3$	20	$58.5*10^3 \pm 60.6*10^3$	20
Volume	μm^3	$66.9*10^3 \pm 12.47*10^3$	20	$235*10^3 \pm 61.5*10^3$	20**
Neuronal soma					
Width	μm	67.96 ± 1.85	31	76.71 ± 2.2	42**
Height	μm	28.95 ± 1.71	25	47.75 ± 2.57	38***
Surface area	μm^2	$32.5*10^3 \pm 2*10^3$	25	$49.1*10^3 \pm 5.3*10^3$	36**
Volume	μm^3	$143*10^3 \pm 19*10^3$	25	$278*10^3 \pm 45.8*10^3$	36**
Axon hillock					
Width of the somal junction	μm	23.1 ± 1.04	27	26.05 ± 0.96	40*
Width of the narrowest part	μm	5.93 ± 0.45	15	4.28 ± 0.34	23**
Axon					
Width	μm	12.54 ± 0.91	19	8.28 ± 0.61	23**
Recurrent dendrite					
Width	μm	4.1 (1 observation only)	1	3.97 ± 0.34	28
Length	μm	261	1	459.3 ± 42.8	28

[1]Results are expressed as means ± SEM. *n* refers to the number of neurons. The statistical significance of the differences, calculated using Student's *t*-test, is given in the last column. where *, **, *** indicate $P < 0.05$, $P < 0.01$, $P < 0.001$, respectively.
*$P < 0.005$.
**$P < 0.01$.
***$P < 0.001$.

accompanied by several thin dendrites extending from the soma (Fig. 4A,B). The remainder of the neurons (38%) had 2–3 main dendrites similar in dimensions (Fig. 4C,E,G). In reference to the pooled data about the physical dimensions of all the neurons: the main dendrite was 85.9 ± 6.1 μm long, and 31.8 ± 1.5 μm wide (n = 25) with a volume and surface area of $66.9*10^3 \pm 12.47*10^3$ μm^3 and $32.9*10^3 \pm 10.6*10^3$ μm^2 (n = 20), respectively (Table 1).

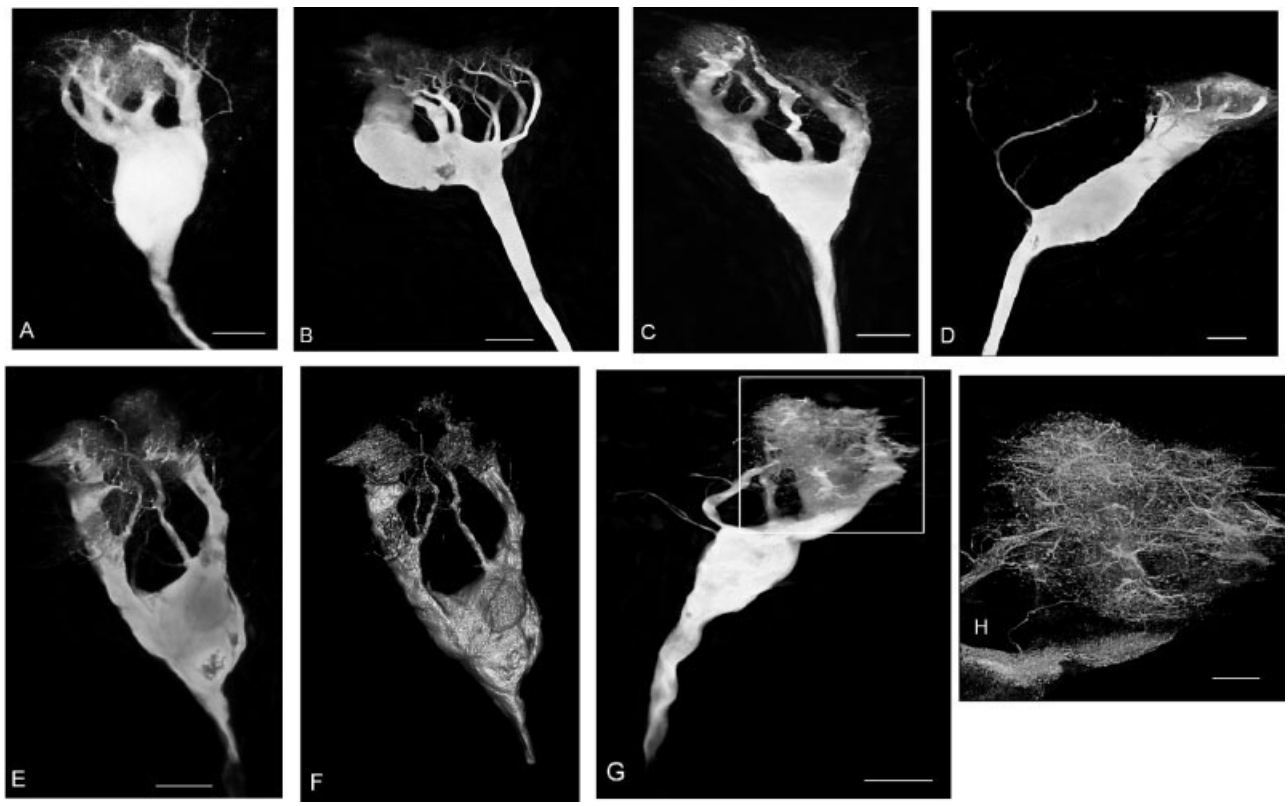

Fig. 4. Fluorescent pictures of some representative types of rapidly adapting neurons (**A–H**). Projection images were reconstructed from a stack of confocal image sections of Alexa hydrazide loaded neurons. F: Surface rendered image of the neuron shown in E. Picture of the fine dendrites of the neuron displayed (in the frame) in G is shown at a larger magnification in H. A–E and G are six different preparations. Scale bars = 50 μm in A–G; 20 μm in H.

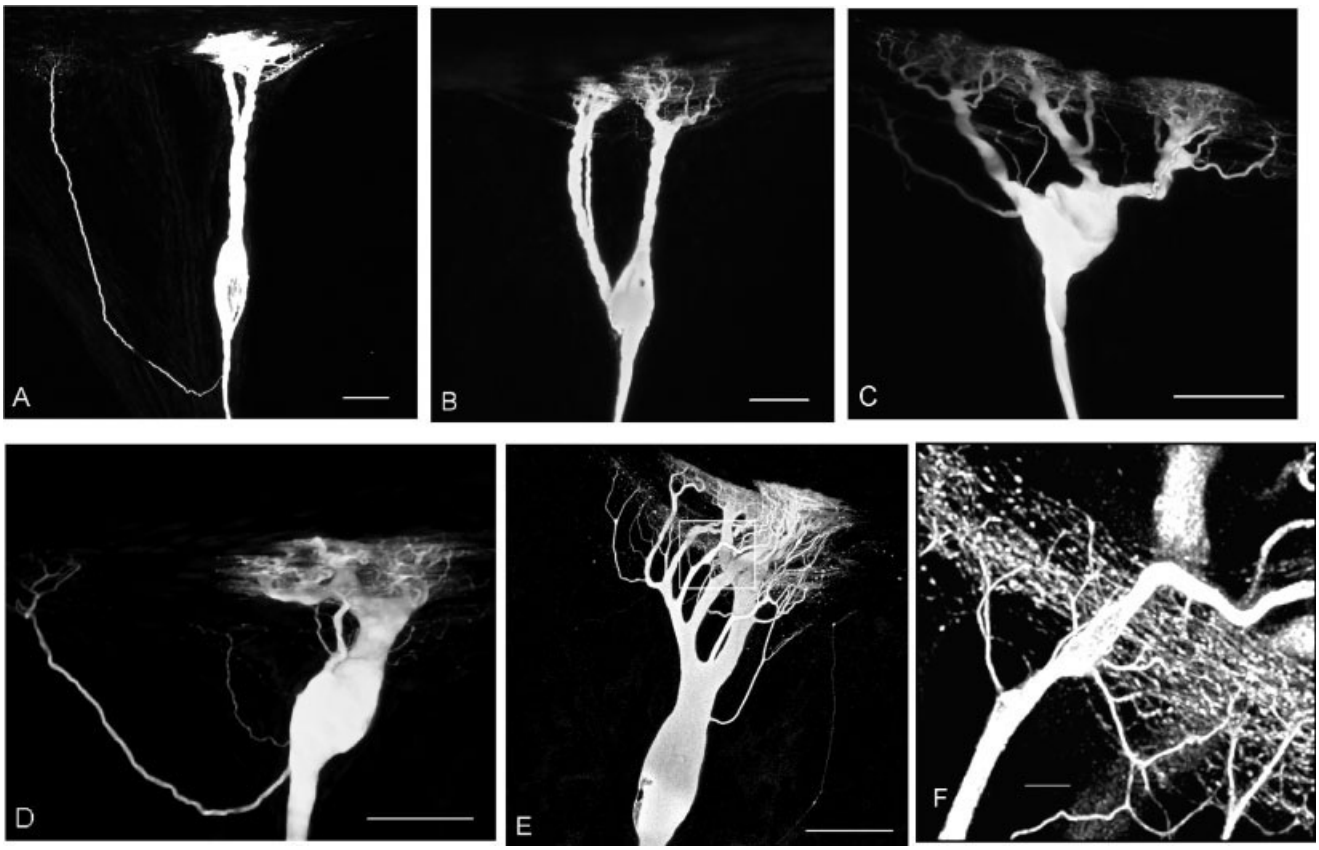

Fig. 5. **A–F:** Fluorescent pictures of some representative types of slowly adapting neurons. Projection images were reconstructed from stack of confocal image sections of Alexa hydrazide-loaded neurons. Picture of a part of the fine dendrites of the neuron displayed (in the frame) in E is shown at a larger magnification in F. Scale bars = 100 μm in A–E; 10 μm in F.

Several short intermediate dendrites originated from the periphery of the main dendrite. Finally, a vast number of thin (0.59 ± 0.05 μm, n = 19) terminal branches, extending from the tips of the intermediate branches to all directions, made a pile of dendrites with a bushy appearance (Fig. 4H). The bushy structure of the terminal dendrites occupied a space of $229*10^3 \pm 38*10^3$ μm^3, 46% of which belonged to the terminal dendrites. A recurrent dendrite, an exceptional type of dendrite originating from the axon hillock, was observed in only 1 out of 31 rapidly adapting neurons examined (Fig. 4D). The central extension from the neuronal soma tapered into a conical structure, giving the axon hillock and, at a further distance, the afferent axon (Fig. 6A). the axon hillock had the largest width, 23.1 ± 1.04 μm (n = 27), at the soma-axonal junction, while at 261 ± 14 μm away from the soma-axonal junction the width gradually decreased to its smallest value, 5.93 ± 0.45 μm (n = 15). The width of the afferent axon at about 1 mm away from cell soma was 12.54 ± 0.97 μm (n = 19) (Table 1).

Slowly adapting receptor neuron

The slowly adapting receptor neuronal soma was located in about the central neighborhood of the slowly adapting receptor muscle. However, compared to the location of the rapidly adapting neurons, the slowly adapting receptor neuronal soma was located away from its receptor muscle (Fig. 1). Receptor neurons lay parallel to the *X-Y* plane. Although some minor variations were observed, a large fusiform somal shape was observed in the many of preparations (Fig. 5). The neuronal surface was not smooth but had many folds and invaginations. The width of the neuronal soma in the *X-Y* plane, 76.71 ± 2.2 μm (n = 42), was larger than that of the rapidly adapting neuron ($P = 3.4*10^{-3}$). The height in the *Z* axis, 47.75 ± 2.57 μm (n = 38), was larger than that measured in the rapidly adapting neuron ($P < 0.0001$). The volume, $278*10^3 \pm 45.6*10^3$ μm^3, and surface area, $49.1*10^3 \pm 5.3*10^3$ μm^2, of the neuronal soma (n = 36) were larger than those calculated in the rapidly adapting neuron ($P = 0.0089$, $P = 0.0055$, respectively) (Table 1).

Peripheral extensions from the soma formed the dendritic tree. Within the slowly adapting neurons an apparent variation was observed in the shape and the dimensions of the dendritic tree (Fig. 5). Neurons could be assigned into five representative groups in reference to the dendritic branching properties (Fig. 5). In 25% of the neurons the soma tapered into a thick, long main dendrite which extended a long distance (about 300 μm) without branching through the connective tissue to the receptor muscle (Fig. 5A). Towards the border of the receptor muscle, 2–5 secondary dendrites extended from the periphery

of the main dendrite and penetrated the receptor muscle. At the insertion region, intermediate dendrites gave many terminal branches. All the neurons in the group had one or more recurrent dendrites originating from the axon hillock. Doubling of the long primary dendrites characterized the main morphological feature of another group of neurons (15%). Both the main dendrites were of similar width (Fig. 5B). Furthermore, the branching properties of the main dendrites were similar to those discussed in the former group. However, none of the neurons in the group had a recurrent dendrite. The volume of the neuronal soma and main dendrite was similar in both groups.

In 23% of the neurons several thin and short dendrites connected the soma to the terminal dendrites (Fig. 5C). Such neurons were relatively small and located very close to the receptor muscle. The mean length of the main dendrite in this group of neurons, 97.1 μm, was similar to that obtained in the rapidly adapting neurons. The mean volume of the soma ($190*10^3$ μm^3), and main dendrites ($104*10^3$ μm^3), of the neurons in the group were smaller than those calculated in the rest of the slowly adapting neurons investigated ($P = 0.047$, $P = 0.03$, respectively).

Eighteen percent of the neurons had a rather thick (27.1 ± 2.6 μm) and significantly shorter (71.8 ± 5.4 μm, $P < 0.0001$) main dendrite as compared to those in the remainder (Fig. 5D). Those neurons received a short recurrent dendrite. Twenty percent of the neurons were observed in various intermediate shapes which could not be sorted into any of the groups defined above (Fig. 5E).

When the data from all the slowly adapting neurons were compiled, the length (179.8 ± 18.1 μm), width (26.3 ± 1.4 μm), and volume ($235*10^3 \pm 61.5*10^3$ μm^3) of the main dendrite of the slowly adapting neuron was significantly different from those of the rapidly adapting neuron ($n = 38$, $P < 0.0001$, $P = 0.0091$, $P = 0.01$, respectively) (Table 1).

Contrary to the apparent morphological variations in the main dendrites the peripheral parts of the dendritic tree had a rather common structure. Two to ten secondary dendrites branched from the main dendrite. The majority of those branched from the periphery of the main dendrite. However, a few dendrites extended from various parts of the main dendrite (Fig. 5C). Secondary dendrites branched 2–4 times and gave intermediate dendrites of various sizes. Those branches penetrated almost perpendicularly into the receptor muscle. The width of the final intermediate branch was 2.42 ± 0.15 μm ($n = 16$). Terminal dendrites bifurcated from the tip of the intermediate branches in both directions in parallel to the receptor muscle fiber. They extended from the parent dendrite almost perpendicularly and gave the characteristic *T pattern* for dendritic termination in the slowly adapting neurons. The width of the terminal dendrites was 0.88 ± 0.09 μm ($n = 16$). Some neighboring terminal branches had dendro-dendritic connections (Fig. 5F). Thus, in all the slowly adapting neurons, dendrites characteristically terminated in the receptor muscle by forming a fine lattice lying parallel to the receptor muscle. In about half of the neurons investigated all the dendrites terminated at a certain location of the receptor muscle (Fig. 5A,D). However, in the rest of the neurons they terminated at multiple sites in the receptor muscle (Fig. 5B,C,E). As shown in Figure 5B,C, terminal dendrites at a certain location extended from a distinct intermediate dendrite. However, in a few neurons an intermediate dendrite supplied branches

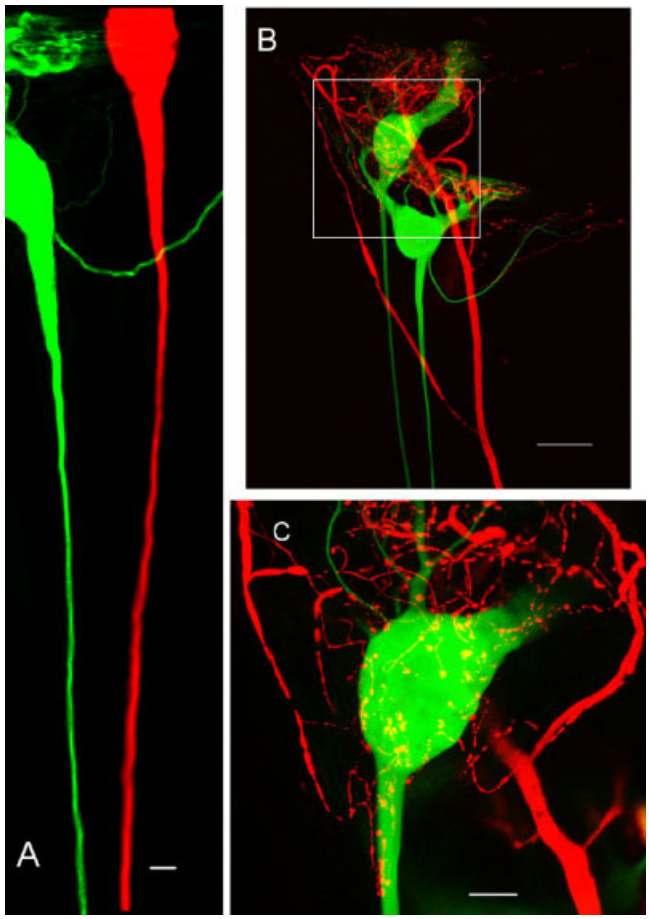

Fig. 6. Images of the fluorescently labeled axons in the stretch receptor preparation. **A:** Afferent axons in fluorescent dye loaded into rapidly (red) and slowly (green) adapting neurons. **B:** Fluorescent image of an efferent axon (red) terminating onto the receptor neurons (green) and muscles. **C:** Section (20 μm in height) of the preparation shown in frame in B imaged at a larger magnification. Scale bars = 25 μm in A,C; 100 μm in B.

to multiple terminal lattices at various locations (Fig. 5E,F). Terminal dendrites occupied a volume of $327*10^3 \pm 56*10^3$ μm^3, 34% of which belonged to the terminal dendrites.

A recurrent dendrite was observed in 66.7% of the slowly adapting neurons investigated. Furthermore, in 15% of the neurons 2–3 recurrent dendrites were present (Figs. 1, 5). Recurrent dendrites originated, as fine branches of the dendrite, mostly from the axon hillock and, in a few neurons, from the axon. They extended to the receptor muscle without branching or a change in width. Many small secondary branches developed from the peripheral part of the recurrent dendrite prior to the insertion into the receptor muscle at a distant location. The mean width and the length of the nonbranching stem of the recurrent dendrite were 3.97 ± 0.34 and 459.3 ± 42.8 μm, respectively ($n = 28$).

The central extension from the neuronal soma tapered into a conical structure and produced an axon hillock and afferent axon with qualitative properties similar to those observed in the rapidly adapting axon (Fig. 6A, Table 1).

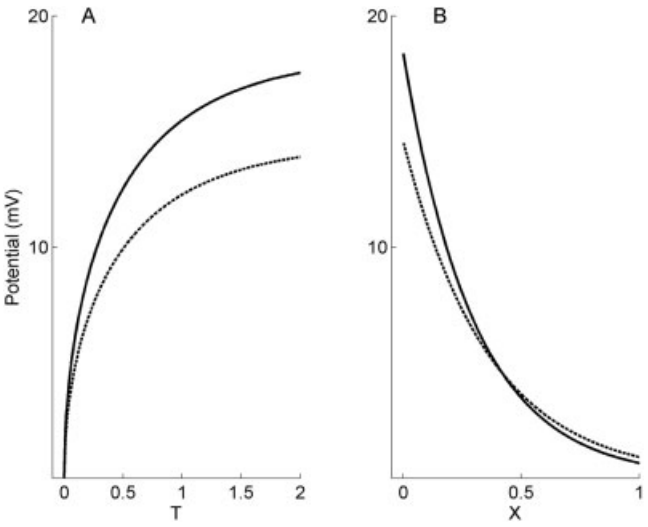

Fig. 7. Calculated potential responses in the main dendrites of the slowly (solid line) and rapidly (dashed lines) adapting main dendrites. Potential responses to 10 nA constant current injection at the site of stimulation **A,** and decay of the responses as a function of distance **B**.

However, the initial width (26.05 ± 0.96 μm, n = 40) and width of the narrowest part of the axonal hillock (4.28 ± 0.34 μm, n = 23) were smaller than those measured in the rapidly adapting neuron ($P = 0.04$, $P = 0.01$, respectively). The axonal width at about 1 mm away from the neuronal soma (8.28 ± 0.61 μm, n = 23) was smaller than that in the rapidly adapting axon ($P = 0.0093$).

Simulation of electrotonic spread of the receptor potential

Physiological consequences of morphological differences between the rapidly and the slowly adapting neurons have been calculated using the cable equation and a computational neuron model simulating the electrotonic spread of the receptor potential.

A major difference between the rapidly and slowly adapting neurons was related to the physical dimensions of the main dendrite. Considering the mean values (Table 1) it was possible to calculate the attenuation of the receptor potential through the main dendrite. Figure 7 shows the calculated charging curves and the steady-state voltage decrement with the distance for both types of main dendrites. The calculated input resistance (R_∞) of the average slowly adapting main dendrite (1.9 MΩ) was larger than that of the rapidly adapting main dendrite (1.4 MΩ). Thus, the same current stimulus (10 nA) induced a larger potential amplitude in the slowly adapting main dendrite at the site of current stimulus than that in the rapidly adapting main dendrite (Fig. 7A). However, the electrotonic decay was faster and took place at a shorter distance in the slowly adapting main dendrite (Fig. 7B). The electrotonic length of the rapidly adapting main dendrite (0.025) was 55% shorter than that of the slowly adapting main dendrite (0. 056). The receptor potential was calculated to attenuate by 2.4% and 5.5% during the electrotonic propagation in the rapidly and slowly adapting main dendrite, respectively.

At the dendro-somal junction the output resistance of the main dendrite, which was also the input resistance of the somal compartment, was calculated according to the following equation:

$$R_\infty = (R_m R_i)^{1/2}/(\pi d^{3/2}) \quad (2)$$

If there was more than one dendrite, the equivalent diameter, d_{eq}, was calculated according to the following equation (Rall and Rinzell, 1973) where all the dendrites were computationally lumped together into a single virtual dendrite at the junction, X_j:

$$d_{eq}(X_j) = [\Sigma_{i=1}^{n}(d_i(X_j)^{3/2}]^{2/3} \quad (3)$$

In the slowly adapting neurons studied, the calculated equivalent diameter and output resistance of the main dendrites was in the range of 27–29 μm and 1.8–1.6 MΩ, respectively.

As shown in Figures 4 and 5, arbitrary branching of the dendrites deviated apparently from that of an idealized neuron; neither dendrites terminated at the same electrotonic distance nor was the 3/2 power rule was satisfied to in branching (Rall, 1959; Rall and Rinzell, 1973). Furthermore, the physical dimensions of the individual neurons differed considerably from the mean values, particularly within the slowly adapting neurons (see Fig. 5). Thus, propagation of the receptor potential could not convincingly be simulated by using mean values and conventional cable equations (Rall, 1959, 1962). Therefore, individual neurons were modeled.

The 3D image of the neuron pair shown in Figure 1B was reduced to a 2D projection. A physical dendrogram (Fig. 8A) was constructed for each neuron by converting the dendrites to the equivalent cylinders. An analogous simplification method was used to produce a single "equivalent dendrite" accurately describing the electrotonic behavior of the dendrites (Clemets and Redman, 1989; Fleshman et al., 1988). The physical dendrogram was converted into the electrotonic dendrogram by assuming appropriate values for R_m and R_i (Fig. 8B). An electrotonic equivalent cable was constructed by lumping together the corresponding parts of the dendritic tree within increments ($\Delta X = 0.004$) of electrotonic distance (Fig. 8C). Thus, at a given electrotonic distance, X_i, the equivalent diameter, $d_{eq}(X_i)$, was calculated according to Eq. 3. The physical length of each sequential cable compartment, i, was calculated using the $d_{eq}(X_i)$ for that compartment and the ΔX:

$$l_i = \Delta X \lambda_i \quad (4)$$

Thus, an equivalent physical cable, with a sequence of compartments of varying diameter, was obtained (Fig. 8D). Rapidly and slowly adapting equivalent cables consisted of a chain of 49 and 77 consecutive compartments, respectively.

Terminal dendrites have been projected into an equivalent compartment and a calculated receptor current with a 30% extension (Fig. 9A) was applied to this compartment (Purali, 2002). In both the rapidly (Fig. 9B) and slowly (Fig. 9C) adapting neuron model, a phase delay and a voltage attenuation was observed when the dendritic receptor potential is compared to the somal receptor po-

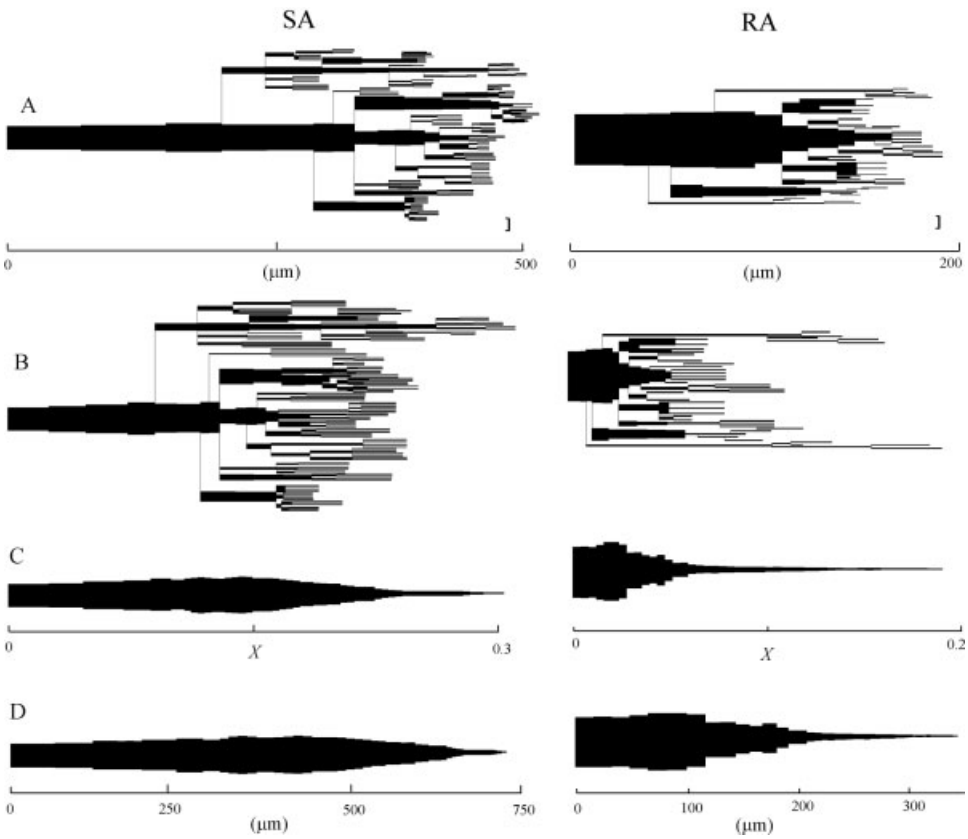

Fig. 8. Embodying neuronal morphology of the receptors in equivalent models. Morphology of the slowly (SA) and the rapidly adapting (RA) receptor neuron pair displayed in Figure 1B has been projected into a 2D physical dendrogram, **A:** Assuming R_m = 10,000Ω cm^2 and R_i = 65Ω cm an electrotonic dendrogram was calculated. **B:** Corresponding parts of the dendrites were computationally lumped together for each increment of electrotonic distance, $\Delta X = 0.004$, to construct the electrotonic equivalent cable. **C:** Finally, a physical equivalent cable of the whole dendritic tree was constructed by calculating the physical length of each compartment. **D:** The slowly and the rapidly adapting neurons were displayed in the left and right columns, respectively. Horizontal axis in B and C are the same; vertical bar is 10 μm.

tential. Dynamic peak amplitude attenuated more than the steady-state level in both models. In the rapidly adapting neuron model the reduction in the dynamic peak and steady-state potential level was 41 and 25%, respectively (Fig. 9B). However, in the slowly adapting model the reduction was larger. Dynamic peak amplitude and steady-state level of the somal potential was 2.5 and 1.8 times smaller than those in the dendritic potential, respectively (Fig. 9C).

Alternatively, sinusoidal current stimulation at various frequencies was used to define the frequency-dependent attenuation in the receptor responses. Voltage attenuation was related to the frequency of the current stimulus (Fig. 9D). If the steady-state voltage attenuation was ignored, the slowly and rapidly adapting dendrites behaved as a sort of low-pass filter with cut-off frequencies at about 20 and 100 Hz, respectively (Fig. 9D).

DISCUSSION

Comparison of the structural properties of the receptor muscles

In the receptor muscles stretch is transformed into tension, which leads to the deformation of the dendrites and gates the mechano-sensitive transducer channels. As a consequence, a receptor current is generated giving rise to receptor potential and impulse responses. Development of a tension response is the principle function common to both receptor muscles. However, it was reported that similar length changes produce different tension responses in the rapidly and the slowly adapting receptor muscles (Ryqvist et al., 1990, 1994). Furthermore, upon stimulation, contraction rates of the slowly and rapidly adapting muscles differ substantially (Fields, 1976). Thus, it is noteworthy to discuss whether morphological differences correlate with the physiological properties of the receptor muscle. Thin myofibrils, with short sarcomeres, are neatly arranged in spiral bundles in the rapidly adapting muscle (Fig. 2). Such properties are typically observed in fast muscle fibers (Jahromi and Atwood, 1967). The muscle fiber is thick and has a spiral shape, supported by a tubulin structure (Fig. 2G). Contrary to the spiral shape of the rapidly adapting muscle, the slowly adapting muscle is flat. Randomly organized thick and flat myofibril bundles of the muscle (Fig. 2) are similar to those of a slow muscle fiber (Jahromi and Atwood, 1967). Thus, the present findings support the notion that the structural differences correlate with the differences in the tension responses (Ryqvist et al., 1990, 1994; Purali, 1997).

The part of the receptor muscles where sensory neuronal dendrites insert has received particular interest since the description of receptors by Alexandrowicz (1951). The region was formerly termed the "intercalated tendon." However, Komuro (1981) used the term "intermediate region" since some myofibrils were shown to pass through the region. In the present study this part of the receptor muscle is named the "neuronal insertion zone" to emphasize the specific function of the region. Florey and Florey (1956) reported that each receptor muscle was composed of several muscle fibers. However, Alexandrowicz (1951,

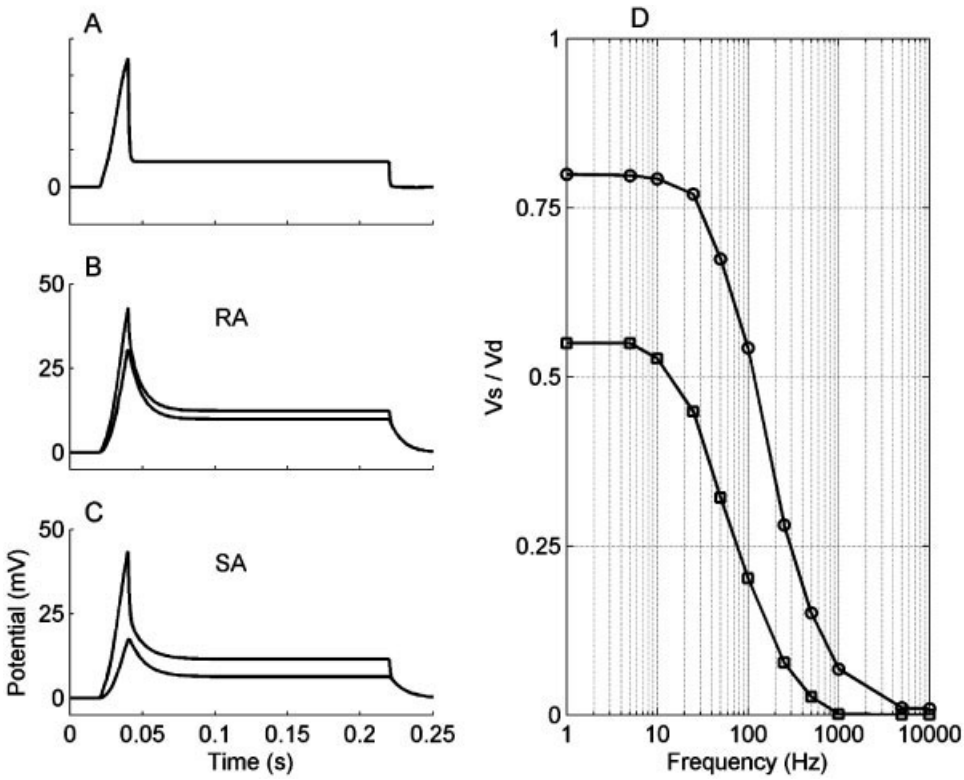

Fig. 9. Comparison of the calculated voltage responses in the transducer dendrites and neuronal soma. The equivalent cables shown in Figure 8 were used to construct a compartmental model of the rapidly and slowly adapting neurons. The terminal dendrites were projected into a single compartment to represent the transducer membrane with the same surface area. Twenty and 61 compartments were assigned for the rapidly and the slowly adapting neuron model, respectively. Calculated receptor current, **A:** was injected into the transducer membrane and the voltage responses were calculated. **B,C:** The superimposed voltage responses at the transducer dendrites and the neuronal soma for the rapidly (RA) and the slowly adapting (SA) neuron models. **D:** The ratio of somal (Vs) to dendritic (Vd) potential responses in the rapidly (circles) and slowly (squares) adapting neuron as a function of the frequency of sinusoidal current stimulation.

1967) described each receptor muscle as composed of, not several muscle fibers, but of bundles of myofibrils which may branch and anastomose. Bodian and Bergman (1962) supported the Floreys' observations, while Fischer et al. (1975) and Komuro (1981) concluded that some muscle fibers run through the muscle fascicle without interruption. Our findings demonstrate that both receptor muscles are single muscle fibers consisting of some subdividing branches. Homogenous diffusion of the injected fluorescent dye within all the receptor muscle compartments indicates that the branches are composed of anastomosing invaginations or extensions of a single plasma membrane (Fig. 2C,D). Furthermore, specific labeling of the myofibrils indicates that branches contain myofibrils passing through the NIZ in both receptor muscles (Fig. 2E). In the slowly adapting muscle, myofibril bundles apparently decrease in thickness as they branch. Some of these branches may be very thin and contain one myofibril. However, they all pass through the NIZ (Figs. 2, 3). Myofibrils terminating in the NIZ were observed only in the rapidly adapting receptor muscle. However, even in the rapidly adapting muscle the majority of myofibril bundles are not interrupted in the NIZ (Figs. 2, 3). In a previous work, Komuro (1981) reported that a small fraction of myofibrils pass through the NIZ. However, the present results demonstrate that interruption of myofibrilar and cytoplasmic continuity is absent in the slowly adapting muscle and very limited in the rapidly adapting muscle. Thus, the present results are partly relevant to the former works investigating NIZ (Alexandrowicz, 1951; Fischer et al., 1975; Komuro, 1981).

It is apparent that the NIZ has a critical importance in the mechano-transduction process. Extensive subdivisions are observed only in the slowly adapting muscle (cf. Fig. 2C,D). This mainly serves to increase the volume of the receptor muscle part housing the terminal dendrites. The major part of the NIZ is occupied by an intercellular matrix filling the space between the intermingling terminal dendrites and muscle branches (Fig. 3E). However, not every muscle branch has a neighboring terminal dendrite, and some dendrites terminate directly into the filling material with no contact with any muscle branch (Fig. 3E). Thus, the filling material should be functioning as an additional viscoelastic element in tension transmission to the terminal dendrites. The length changes in the slowly adapting receptor muscle should correlate well with a length change in the NIZ. Uniformly distributed parallel myofibril bundles should transmit and maintain a sustained and evenly distributed tension response which deforms the NIZ and eventually the terminal dendrites in the direction of the length change. However, the volume of the NIZ is larger than the volume of an equal length of slowly adapting muscle and the density of the myofibrils in the NIZ is low (Figs. 2, 3). It is conceivable that the tension response to length change would be transmitted to the NIZ with a time delay, which would attenuate the sensed amplitude if the stimulus frequency is high.

In contrast, in the rapidly adapting receptor the NIZ is composed of a lobe of fine dendrites, embedded into a mass of connective tissue located within spiral muscle branches (Fig. 3A). The volume of the muscle fiber is similar to that of the lobe, indicating that the muscle fiber could drive the mechanical properties of the lobe dynamically. Such an apparatus may effectively couple the receptor muscle extension to deformation of dendrites even when the stimulus frequency is high. Receptor muscle extension would

produce a rotation and extension deforming the lobe. Multidirectional forces, deforming the bushy dendrites, may well be the cause of the hump observed in the tension responses to the short range of muscle extensions (Rydqvist et al., 1994). Thus, morphological properties of the NIZ in both receptor muscles are relevant to the viscoelastic properties of the receptor muscle fibers (Rydqvist et al., 1990, 1994), and contribute significantly to the receptor responses (Purali, 1997).

Comparison of the structural and electrotonic properties of the receptor neurons

Mechano-electrical transduction is the most specialized feature of this sense organ. Alexandrowicz (1951) proposed that this event should take place in the fine dendrites of the receptor neurons. Tao-Cheng et al. (1981), using electron microscopy, concluded that the dendritic tip membrane might be the region where receptor potential is produced. However, Erxleben (1989), using patch-clamp technique, reported that mechano-sensitive transducer channels are present in the main dendrite and cell soma of the receptor neurons. Thus, the transducer current could also be generated at those sites. At present, it is not possible to compare the relative magnitude of the transducer current evoked at those sites to that generated in the terminal dendrites, since the density distribution of the transducer channels in the neuronal membrane has not yet been explored. What is known is that in both receptor neurons a large volume of terminal dendrites are present with a comparable surface area to that of the main dendrite or neuronal soma. Furthermore, receptor muscle extension evokes the maximum deformation specifically in the terminal dendrites. Thus, terminal dendrites of the receptor neurons should be the primary elements where mechanical stimulus is converted into ionic current even when a homogeneous transducer channel distribution is presumed.

Terminal dendrites occupy a similar space in both receptor neurons. However, a major difference is observed in their shape and location, which may influence their function. In the slowly adapting neuron the *T*-shaped bifurcation of the terminal dendrites, and their longitudinal insertion into the receptor muscle, correlate with the morphological properties of the NIZ (Fig. 5F). The thin and long terminals enable a specific selectivity to sense the length changes over a broad range with high precision. However, potential signals might be attenuated significantly in long dendrites. The electrotonic length *(L)* increases as the thickness decreases. Thus, in a 33-μm long terminal dendrite, during the electrotonic transmission from dendrite tip to the bifurcation point, the receptor potential would be attenuated at a similar magnitude to that which takes place throughout the main dendrite (l = 180 μm). However, the connections between the longitudinal dendrite branches create a lattice which increases the conductance of the terminal dendrites and facilitates the passive propagation of the receptor potential (Fig. 5). Thus, in response to a mechanical stimulation, by the concerted action of each terminal dendrite unit, an evenly distributed receptor potential would be generated in the fine dendritic lattice.

In the rapidly adapting neuron a similar volume of terminal dendrites are concentrated in a lobe of connective tissue located within the curls of the receptor muscle (Figs. 3A, 4). The physical and electrotonic length of the terminal dendrites are considerably shorter than those in the slowly adapting neuron. Thus, the receptor potential propagates with less attenuation compared to that in the slowly adapting neuron.

In both receptor neurons the terminal dendrites are connected to the main dendrite via some intermediate dendrites of various sizes. An apparent difference is observed in the shape of the main dendrites. The diversity is more pronounced in the slowly adapting neurons as compared to that in the rapidly adapting neurons (cf. Figs. 1, 4, 5). Considering the mean results (Table 1) the main dendrite of the slowly adapting neuron is 21% thinner and 2.1 times longer. In Figure 7A,B the calculated charging curves and the steady-state voltage decrement with distance are shown for both main dendrites. Due to the smaller diameter the input resistance of the slowly adapting main dendrite is 35% larger than that of the rapidly adapting main dendrite. Thus, the same current stimulation evokes a larger potential amplitude at the injection site ($X = 0$). However, the small diameter increases the axonal resistance and causes larger voltage decrement at shorter distances (Fig. 7B). Furthermore, the electrotonic length (L) is 2.2 times longer compared to that of the rapidly adapting main dendrite. Thus, receptor potential is calculated to attenuate 2.4% and 5.5% during the electrotonic propagation in the rapidly and the slowly adapting main dendrite, respectively. The calculated results indicate that in both receptor neurons the main dendrites transmit the steady-state receptor potential with a small attenuation. However, it should be emphasized that those calculations are for constant current injection in an infinite cable, and attenuation is amplified if the applied current changes with time. For a 100 Hz AC current stimulation, the calculated nonsteady length constant, λ_{AC}, would be 48% shorter than λ_{DC}, and would induce 4.6% and 10.3% voltage attenuation in the rapidly and the slowly adapting main dendrites, respectively.

Calculations indicate that the rapidly adapting main dendrite conducts the receptor potential to the soma with a low percent of attenuation. Although the calculations have been made according to the mean values from all experiments, the results could be generalized to all neurons, since the variation in the length and width of the rapidly adapting main dendrites is very limited (Fig. 4). On the contrary, significant voltage attenuation is calculated in the slowly adapting main dendrite. Furthermore, variation in the length and width of the main dendrite is very large (Fig. 5). The longest dendrite, which is 505 μm, would evoke 15.5% and 27.8% voltage attenuation for steady-state and 100 Hz AC current stimulation, respectively.

The cross sectional area of the main dendrite(s) defines the input conductance of the somal compartment at the dendro-somatic junction (see Eq. 2). As can be followed in Figures 4 and 5, various types of dendrites are observed. Variation is particularly apparent in the slowly adapting receptor neuron. The width of the main dendrites in Figure 5A,D are both ~28 μm. Thus, both main dendrites are coupled to the receptor neurons through similar input resistances. However, neurons in Figure 5B,C have more than one main dendrite. In this case the calculated equivalent diameter, d_{eq}, representing all the main dendrites, could be used for comparison (Rall and Rinzell, 1973).

Such a calculation gives 28 μm, for the three main dendrites in Figure 5C, and 29 μm for the two main dendrites in Figure 5B, indicating a similarity in the input conductance of the neurons even when multiple main dendrites are present.

Beyond the dendro-somal junction the dendrite enlarges considerably and becomes the neuronal soma. Considering the nongeometrical shape (Figs. 4, 5), it is not possible to fit an equation properly representing the electrotonic properties of the soma. However, on the basis of surface area measurements some discussion is possible. As a biological cable the soma is the best conducting part of the receptor neuron, since it has the largest cross-sectional area. However, the soma is the leakiest compartment. Considering the mean volume and surface measurements, the volume/surface ratio of the rapidly and slowly adapting soma is 4.4 and 5.6, respectively (Table 1). This is much lower than that calculated for a sphere with the measured mean diameter. It is possible to propose that both the irregular shape and surface folding (see Fig. 4F) decrease the conductance of the soma considerably. Thus, a part of the receptor current generated in the terminal dendrites would flow across the somal membrane. The somal surface area of the slowly adapting neuron is larger by a factor of 1.51 compared to that of the rapidly adapting neuron (Table 1). Thus, an additional 51% current stimulus would be needed to charge the slowly adapting soma to the same potential as the rapidly adapting soma. In physiological conditions the current stimulus is the receptor current which flows from terminal dendrites through the dendritic tree to the soma (Brown et al., 1978; Rydqvist and Purali, 1993). Considering the electrotonic properties, for a given stimulation (i.e., receptor muscle extension) a slowly adapting soma is estimated to depolarize less compared to that which takes place in the rapidly adapting soma. The electrotonic voltage attenuation, evoked by the somal membrane, should particularly be important in the rapidly adapting neuron, where action potentials are initiated in the initial part of the axon (Purali, 1997; Purali and Rydqvist, 1998). As shown in Figure 4B, the rapidly adapting soma contracted to a smaller size probably to reduce the attenuation.

By using the mean values and the conventional cable equations (Rall, 1959, 1962) passive properties of the receptor neurons could only be partly simulated. For example, the diameter of the thick main dendrites of the neurons shown in Figure 5A,D are both about 28 μm. They are 25–33% thicker than the diameter of any main dendrites of the neurons shown in Figure 5B,C. However, the calculated equivalent diameters of the dendrites in Figure 5B,C are 29 and 28 μm, respectively. Thus, the equivalent diameter of the slowly adapting main dendrite is larger than the mean of the measurements. Therefore, a realistic model, taking arbitrary branching and anatomic variations into consideration, is required to improve the fidelity of the simulations. In the present work, as a representative example, the receptor neuron pair shown in Figure 1B was modeled. Using 3D images, physical and electrotonic dendrograms were constructed (Fig. 8A,B). At this stage it is possible to construct a compartmental neuron model, where each segment uniquely specifies the location of each compartment in the electrical circuit representing the topology of the original neuron (Nitzan et al., 1990). However, in that case the number of compartments would increase to several hundreds. Thus, the analogs simplification method (Clemets and Redman, 1989; Fleshman et al., 1988) supplied a reliable alternative by reducing both the geometrical complexity and number of compartments (Fig. 8D).

In both the rapidly and slowly adapting model, the dynamic and steady parts of the potential responses attenuated significantly when a calculated current stimulus was used (Fig. 9A–C). As compared to those obtained by conventional calculations the attenuation in the complete neuron model is much larger. The passive properties of neuronal soma and the intermediate dendrites, represented in the complete neuron model, should be the cause of the difference. Contrary to the short physical length, the electrotonic length of the intermediate dendrites may be comparable to that of the main dendrites, since their diameter is quite small (see Fig. 8B). The neuronal soma is another cause of the attenuation. However, the somal size of the neuron pair used in the simulations differs by about 11%; therefore, the cause of further differences should stem from the variations in the dendritic morphology. It should be emphasized that the intermediate dendrites, main dendrite(s), and soma lie in series from the primary transducer site, terminal dendrites, to the impulse initiation site, axon hillock. The controlled parameter in biology and in the model is the receptor current generated in the terminal dendrites. Thus, the membrane potential changes are defined by the current clamp conditions. In consequence, an increase in the size of the soma would not only reduce the somal potential response, but also the receptor potential in the primary transducer will be reduced even though the stimulus is the same.

The electrotonic voltage attenuation is related to the frequency of the current stimulus (Fig. 9D). The slowly and rapidly adapting dendrites constitute a type of low-pass filter with cut-off frequencies at about 20 and 100 Hz, respectively (Fig. 9D). The thick and short dendritic structure of the rapidly adapting neuron enables rapid propagation of the receptor potential. Furthermore, properties of the electrotonic filter fit well with the firing capacity of the receptor neuron, which could fire more frequently than 100 Hz (Purali, 2002). Thus, rapid changes in the dendritic potential could be converted into neural activity in the soma (or axon hillock) with a small attenuation, as expected from a dynamic receptor. These properties are compatible with the morphological properties of the rapidly adapting receptor muscle discussed above. In contrast, the thin and long dendritic structure of the slowly adapting neuron attenuates and slows down the electrotonic propagation of the dendritic potential to the soma. In response to an incremental increase in the receptor muscle length, due to the passive properties of the dendritic pathway, the duration and amplitude of the dendritic potential response would be represented in finer increments of receptor potential in the soma. Thus, only sufficiently large and/or long changes in the dendritic potential would be converted into neural activity. Flattening of the transient peak and reduction of the steady part of the response may contribute to the slow adaptation in the neuron by preventing the depolarization block, responsible for the termination of the impulse responses (Purali, 1997, 2002; Purali and Rydqvist, 1998). The electrotonic properties of the slowly adapting neuron are relevant to the morphological properties of the slowly adapting receptor muscle discussed above.

In a former study, using somal electrodes, Rydqvist and Purali (1993) reported that in the slowly adapting neuron the amplitude of the receptor current was smaller and flattening of the initial peak amplitude was more apparent compared to those in the rapidly adapting neuron. The differences may partly stem from the visco-elastic properties of the receptor muscles (Rydqvist et al., 1994). However, considering present recordings and calculations, differences in neuronal morphology may have a significant role in the genesis of the reported differences (Fig. 9B,C).

A recurrent dendrite has been observed in the majority of slowly adapting neurons investigated. In relation to the mean length and diameter (459 and 3.97 μm), the potential contribution of a recurrent dendrite to receptor responses would be much fainter compared to those of the principle dendrite.

The central extension from the neuronal soma gives the axon hillock and the afferent axon. The surface area of the axon hillock is comparable to that of the soma. Thus, the specific shape of the axon hillock may serve to increase the amount of current directed into the axonal compartment (Fig. 6A). Considering the equation $\theta = 2\lambda/\tau m$, giving the conduction velocity in a tubular axon, and the 51% difference between the axonal diameters, we find the calculated conduction velocity is 23% faster in the rapidly adapting axon. This is compatible with the other properties of the neurons discussed above.

The present work demonstrates that the morphology of the rapidly and slowly adapting neurons might have evolved to construct a sort of biological filter to optimally sense the dynamic and the static features of the mechanical stimulus, respectively. Future studies should focus on the investigation of the density and topographical distribution of the voltage-gated and mechano-sensitive ionic channels.

ACKNOWLEDGMENT

I thank Prof. S. Yorukan for reading the article.

LITERATURE CITED

Alexandrowicz JS. 1951. Muscle receptor organs in the abdomen of *Homarus vulgaris* and *Palinurus vulgaris*. J Microsc Sci 92:163–200.

Alexandrowicz JS. 1967. Receptor organs in thoracic and abdominal muscles of Crustacea. Biol Rev 42:288–326.

Bodian D, Bergman RA. 1962. Muscle receptor organs of the crayfish: functional and anatomical correlations. Bull Johns Hopkins Hosp 110: 78–106.

Brown HM, Ottoson D, Rydqvist B. 1978. Crayfish stretch receptor: an investigation with voltage-clamp and ion-sensitive electrodes. J Physiol 284:155–179.

Clemets JD, Redman S. 1989. Cable properties of cat spinal motoneurons measured by combining voltage clamp, current clamp and intracellular staining. J Physiol 409:63–87.

Diaz JF, Strobe R, Engelborghs Y, Souto AA, Andreu JM. 2000. Molecular recognition of taxol by microtubules. Kinetics and thermodynamics of binding of fluorescent taxol derivatives to an exposed site. J Biol Chem 275:26265–26276.

Erxleben C. 1989. Stretch-activated current through single ion channels in the abdominal stretch receptor organ of the crayfish. J Gen Physiol 94:1071–1083.

Fields HL. 1976. Crustacean abdominal and thoracic muscle receptor organs. In: Mill PJ, editor. Structure and function of proprioceptors in the invertebrates. London: Chapman and Hall. p 65–114.

Fischer W, Fisher H, Uerlingo I, David H. 1975. Licht und electronenmikroskopishe Untersuchungen an den langsam adaptierenden abdominalen Dehnungsrezetoren des amerikanishen Fluss Krebses *Orconectes limosus* (RAF). Z Microsk Anat Forsch 89:340–366.

Fleshman JW, Segev I, Burke RE. 1988. Electrotonic architecture of type-identified alpha-motoneurons in the cat spinal cord. J Neurophysiol 60:60–85.

Florey E, Florey E. 1956. Microanatomy of the abdominal stretch receptors of the crayfish (*Astacus fluviatilis*). J Gen Physiol 39:69–85.

Frey T. 1995. Nucleic acid dyes for detection of apoptosis in live cells. Cytometry 21:265–274.

Jahromi SS, Atwood HL. 1967. Ultrastructural features of crayfish phasic and tonic muscle fibres. Can J Zool 45:601–606.

Johnston D, Mia-Sin WD. 1995. Functional properties of dendrites. In: Johnston D, Mia-Sin WD, editors. Foundations of cellular neurophysiology. Cambridge, MA: MIT Press. p 55–109.

Koch C, Segev I. 1998. Cable theory for dendritic neurons. In: Koch C, Segev I, editors. Methods in neuronal modeling. Cambridge, MA: MIT Press. p 28–136.

Komuro T. 1981. Fine structural study of the abdominal muscle receptor organs of the crayfish (*Procambarus clarkii*). Fast and slow receptor muscles. Tissue Cell 13:79–92.

Nitzan R, Segev I, Yarom Y. 1990. Voltage behavior along the irregular dendritic structure of morphologically and physiologically characterized vagal motoneurons in the guinea pig. J Neuropysiol 63:333–346.

Purali N. 1997. Mechanism of adaptation in a mechanoreceptor. A study of mechanical and ionic factors in the crayfish stretch receptors. Stockholm: Repro Print.

Purali N. 2002. Firing properties of the soma and axon of the abdominal stretch receptor neurons in the crayfish (*Astacus leptodactylus*). Gen Physiol Biophys 21:205–226.

Purali N, Rydqvist B. 1992. Block of potassium outward currents in the crayfish stretch receptor neurons by 4-aminopyridine, tetraethylammonium chloride and some other chemical substances. Acta Physiol Scand 146:67–77.

Purali N, Rydqvist B. 1998. Action potential and sodium current in the stretch receptor neurons in the crayfish. J Neurophysiol 80:2121–2132.

Rall W. 1959. Branching dendritic trees and motoneuron membrane resistivity. Exp Neurol 1:491–527.

Rall W. 1962. Theory of biophysical properties of dendrites. Ann N Y Acad Sci 96:1071–92.

Rall W, Rinzel J. 1973. Branch input resistance and steady attenuation for input to one branch of a dendritic neuron model. Biophys J 13:648–688.

Rydqvist B, Purali N. 1991. Potential-dependent potassium currents in the rapidly adapting stretch receptor neuron of the crayfish. Acta Physiol Scand 142:67–76.

Rydqvist B, Purali N. 1993. Transducer properties of the rapidly adapting stretch receptor neuron in the crayfish (*Pacifastacus leniusculus*). J Physiol 469:193–211.

Rydqvist B, Swerup C, Lannergren J. 1990. Visco-elastic properties of the slowly adapting stretch receptor muscle of the crayfish. Acta Physiol Scand 139:519–527.

Rydqvist B, Purali N, Lannergren J. 1994. Visco-elastic properties of the rapidly adapting stretch receptor muscle of the crayfish. Acta Physiol Scand 150:151–159.

Schiemann T, Bomans M, Tiede U, Höhne K-H. 1992. Interactive 3-D segmentation of tomographic image volumes. 14. DAGM symposium Mustererkenung. Berlin: Springer. p 73–80.

Swerup C, Rydqvist B. 1992. The abdominal stretch receptor organ of the crayfish. Comp Biochem Physiol 103A:423–431.

Tao-Cheng JH, Hirosawa K, Nakajima Y. 1981. Ultrastructure of the crayfish stretch receptor in relation to its function. J Comp Neurol 200:1–21.

van Harreveld A. 1936. A physiological solution for freshwater crustaceans. Proc Soc Exp Biol 34:428–432.

Waterman-Storer C, Duey DY, Weber KL, Keech J, Cheney RE, Salmon ED, Bement WM. 2000. Microtubules remodel actomyosin networks in *Xenopus* egg extracts via two mechanisms of F-actin transport. J Cell Biol 150:361–376.